Exosomes derived from human adipose-derived stem cells ameliorate osteoporosis through miR-335-3p/Aplnr axis

Chunhui Sheng[1,§], Xiaodong Guo[1,§], Zhuqing Wan[1], Xiaoqiang Bai[1], Hao Liu[1], Xiao Zhang[1], Ping Zhang[1], Yunsong Liu[1], Wenyue Li[2] (✉), Yongsheng Zhou[1] (✉), and Longwei Lv[1] (✉)

[1] *National Center of Stomatology & National Clinical Research Center for Oral Disease, National Engineering Research Center of Oral Biomaterials and Digital Medical Devices, Beijing Key Laboratory of Digital Stomatology, Key Laboratory of Digital Stomatology, Department of Prosthodontics, Peking University School and Hospital of Stomatology, Beijing 100081, China*
[2] *Department of Stomatology, Beijing Chao-Yang Hospital, Capital Medical University, Beijing 100020, China*
§ *Chunhui Sheng and Xiaodong Guo contributed equally to this work.*

ABSTRACT

Treatment of osteoporosis is still a challenge in clinic, which leads to an increasing social burden as the aging of population. Exosomes originated from human adipose-derived stem cells (hASCs) hold promise to promote osteogenic differentiation, thus may ameliorate osteoporosis. The main purpose of this study was to investigate the novel usage of hASC-derived exosomes in the treatment of osteoporosis and their underlying mechanism. Two types of exosomes, i.e., exosomes derived from hASCs cultured in proliferation medium (P-Exos) and osteogenic induction medium (O-Exos), were obtained. As compared with P-Exos, O-Exos could promote the osteogenic differentiation of mouse bone marrow-derived stem cells (mBMSCs) from osteoporotic mice *in vitro* and ameliorated osteoporosis *in vivo*. Then, microRNA (miRNA)-335-3p was identified to be the key differentially expressed microRNA between the two exosomes by small RNA sequencing, gene overexpression and knock-down, qRT-PCR, and dual-luciferase reporter assay, and Aplnr was confirmed to be the potential target gene of miRNA-335-3p. In addition, miR-335-3p inhibitor-optimized O-Exos were established by transfection of miR-335-3p inhibitor, which significantly enhanced the osteogenic differentiation of mBMSCs *in vitro*, and bone density and number of trabecular bones *in vivo* compared with unoptimized O-Exos. Our results indicated that the ASC-exosome-based therapy brings new possibilities for osteoporosis treatment. Besides, engineered exosomes based on transfection of miRNA are a promising strategy to optimize the therapeutic effect of exosomes on osteoporosis.

KEYWORDS

osteoporosis, adipose-derived mesenchymal stem cells, exosomes, microRNA, osteogenic differentiation

1   Introduction

Osteoporosis is a common disease in the middle-aged and elderly population, which has a huge impact on the quality of life. At present, the number of people aged 50 years and older suffering osteoporosis or at risk because of low bone mass is approximately 54 million in the United States [1], while in China about 60 million people have osteoporotic problems [2]. As the aging of population, social burden caused by osteoporosis increased year by year [3, 4]. Nowadays, the treatment of osteoporosis mainly depends on drugs, including bisphosphonates, anti-RANKL antibody, and hormone (estrogen or parathyroid hormone) [5]. However, these kinds of drugs were still associated with several side effects, such as the necrosis of jaws [6] and risk of thromboembolic events [7]. Thus, researchers have devoted to developing new safer methods for anti-osteoporosis therapy.

Mesenchymal stem cells (MSCs) are undifferentiated cells with self-renewal and multi-lineage differentiation ability, which endows them the potential to be used in regenerative medicine and the treatment of diseases. A series of studies have confirmed

the beneficial effect of bone marrow-derived MSCs (BMSCs) on improving the osteoporotic conditions [8]. Besides, local infection of adipose-derived MSCs (ASCs) has also been proved to have beneficial effect to improve the bone quality of osteoporotic mice [9]. However, the potential risk of tumorigenesis, unwanted immune responses, and other risks of stem cell therapy have limited its clinical application [10].

Exosomes are one kind of cell-secreted extracellular vesicles with a diameter between 40–160 nm, which participate in a variety of physiological and pathological processes by delivering biological molecules, such as proteins, nucleic acids, and transcription factors to recipient cells [11, 12]. In recent years, due to its lower immunogenicity, safer, and easier for storage or delivery [11] compared with stem cell therapy, exosome-based cell-free therapy has been of increased interest in tissue regeneration and disease treatment, such as bone regeneration [13] and acute respiratory distress syndrome [14]. BMSC-derived exosomes have been widely explored to facilitate osteogenic differentiation [15, 16]. However, BMSCs are difficult to obtain and may cause tissue defects in the donor sites, which limits the possibility of their large-

scale clinical application. In contrast, ASCs have the advantages of good accessibility (e.g., by liposuction and extracted from discarded adipose tissue), abundant quantities, and less donor pain [17, 18]. Besides, ASCs are highly efficient exosome-secreting cells with strong proliferation and osteogenic differentiation potential. Thus, from the perspective of clinical application, ASCs are more ideal exosomal donor cells. In fact, ASC-derived exosomes have been confirmed to have the effect of promoting osteogenic differentiation of BMSCs *in vitro* and osteogenesis *in vivo* [19]. However, the effect of human ASC (hASC)-derived exosomes on the osteogenic differentiation ability of osteoporotic BMSCs and their preventive effect on osteoporotic bone loss are still largely unknown.

Several studies have suggested that exosomes could inherit the properties of their host cells [20, 21]. In this study, exosomes derived from hASCs cultured in osteogenic medium (O-Exos) were obtained to investigate their effect on the osteogenic capacity of BMSCs under osteoporotic condition and application in the treatment of osteoporosis, while exosomes derived from hASCs cultured in proliferation medium (P-Exos) were used as the control. Moreover, the key different microRNA (miRNA) encapsulated in the hASC-derived exosomes and its target gene were identified via miRNA sequencing, gene knock-down and overexpression, and dual-luciferase reporter assay to understand the underlying mechanism by the exosomes to stimulate osteogenesis. In addition, we further evaluated the effect of the optimized exosomes by transfection of the key miRNA inhibitor on osteogenic differentiation *in vitro* and osteoporosis *in vivo*.

2 Experimental

2.1 Cell culture and osteogenic induction

The hASCs were purchased from ScienCell Research Laboratory (CA, USA) and the mouse BMSCs (mBMSCs) were purchased from Procell (Wuhan, China). Besides, primary mBMSCs from osteoporotic mice (OVX mBMSCs) were isolated, the method of which was described in Section 2.3. The cells were cultured in the following conditions: 37 °C temperature, 5% CO_2 atmosphere, and full relative humidity. hASCs were expanded in proliferation medium (PM) consisted of Dulbecco's modified Eagle's medium (DMEM, Gibco, NY, USA), 10% (v/v) fetal bovine serum (FBS) (ScienCell, USA), 100 U/mL penicillin G, and 100 mg/mL streptomycin (Gibco, NY, USA). Same proliferation medium was used for mBMSCs expansion, except that DMEM was replaced by minimum essential medium α (α-MEM, Gibco, Grand Island, USA).

To induce osteogenic differentiation, the medium of hASCs or mBMSCs was replaced by osteogenic induction medium (OM) consisted of PM plus 10 nM dexamethasone, 10 mM β-glycerophosphate, and 0.2 mM ascorbic acid, when the cells reached 70%–80% confluence. All other materials were purchased from Sigma-Aldrich (MO, USA) unless otherwise stated.

2.2 Animal model

Six-week-old female BALB/c mice were purchased from Vital River Corporation (Beijing, China). The animal study was approved by the Institutional Animal Care and Use Committee of the Peking University Health Science Center (LA2019019). The mice were raised in an environment with a constant temperature of 25 °C and 12-h light/dark cycle, and fed with unlimited food and water. After two weeks, the mice were randomly divided into two groups for ovariectomy (OVX) or sham operation, respectively. All the surgery were performed under general anesthesia by intraperitoneal injection of pentobarbital sodium

with buprenorphine for analgesia. Briefly, in the OVX group, an approximately 5 mm incision was created in the middle of the abdominal skin, the uterus was then found with blunt separation, along the fallopian tubes, then both ovaries were exposed and excised. In the sham group, the ovaries were exposed in the same way, but not removed. Then, the skin was sutured, and the mice were kept in a warm environment until they waked up.

2.3 Isolation and expansion of primary OVX mBMSCs

In brief, the mice were sacrificed 12 weeks after the surgery, and their femurs were collected. Then, both ends of the femurs were cut off and the bone marrow was flushed out with α-MEM added with 10% (vol/vol) FBS. After cultured for 24 h, the supernatants were discarded, and the adherent cells were continued to be cultured until 70%–80% confluence with medium refreshed every 2 or 3 days. The culture conditions and methods of osteogenic induction were the same as mBMSCs. Cells of passage 2 were used for following studies.

2.4 Exosome isolation and characterization

FBS was first ultra-centrifugated (Optima L8-80XP, Beckman Coulter, CA, USA) for 16 h at 100,000*g* to deplete bovine exosomes. When hASCs arrived at 80% confluence, the culture medium was replaced with PM or OM containing FBS depleted of exosomes. Then, the supernatants were harvested every 72 h for exosome isolation. In detail, the supernatants were first centrifuged at 2,000*g* for 20 min [19], then 10,000*g* for 40 min, and 100,000*g* for 70 min after filtered through a 0.22-μm sterilized filter (Merck Millipore, Darmstadt, Germany). The pellets were resuspended in PBS followed by another ultracentrifugation at 100,000*g* for 70 min to obtain the pelleted exosomes, which were resuspended in 200 μL PBS for further assays. The concentration of exosomes was then quantified by a Pierce bicinchoninic acid (BCA) protein assay kit (Thermo Scientific, MA, USA) as per the manufacturer's instructions.

The morphology of exosomes was detected by the transmission electron microscopy (TEM). In detail, P-Exos or O-Exos were fixed in 2% paraformaldehyde for 30 min and then dropped on copper grids coated with carbon. A negative staining of the mixture with 1% uranyl acetate was conducted twice. Images were captured using JEM1400PLUS (JEOL, Tokyo, Japan) at 120 kV.

The size distribution of the collected exosome particles was determined by the nanoparticle tracking analysis (NTA, ZetaVIEW S/N 17-310, Particle Metrix, Bavaria, Germany), and the data were analyzed with NTA analytical software (ZetaView 8.04.02, Particle Metrix, Bavaria, Germany).

Western blotting was used to identify the markers of exosomes, including: CD9 (ab92726, Abcam, Cambridge, UK), CD81 (ab79559, Abcam, Cambridge, UK), TSG101 (ab125011, Abcam, Cambridge, UK), and β-tubulin (Abcam, Cambridge, UK). The detailed procedures were described in Section 2.13.

2.5 Cellular internalization of exosomes

Firstly, exosomes were labeled with PKH26 (Umibio, Shanghai, China) as per the manufacturer's directions. Then, the labeled exosomes were resuspended in PBS and then incubated with mBMSCs for 12, 24, 48, and 72 h, respectively. At the indicating timepoint, the cells were rinsed with PBS and fixed in 4% paraformaldehyde at room temperature for 10 min. After washing with PBS, the cell nuclei were stained with 4,6-diamidino-2-phenylindole (DAPI). Images were captured by a confocal laser scanning microscope (TCS-SP8 STED 3X, Leica, Wetzlar, Germany). Quantitative analysis was achieved by calculating the integrated density of red fluorescence through ImageJ software (https://imagej.net).

2.6 miRNA expression profile by RNA sequencing

Total RNAs of P-Exos and O-Exos were isolated with miRNeasy Maxi Kit (QIAGEN, Dusseldorf, Germany). Small RNA libraries were constructed using QIAseq miRNA Library Kit (QIAGEN, Dusseldorf, Germany). Sequencing was performed on a HiSeq 2000 (Illumina, CA, USA), and the data were collected and analyzed using a data collection software (Illumina, CA, USA). Differential miRNA expression presenting a $\log_2$(fold change) ($\log_2$FC) ≥ |1| was identified as differentially expressed miRNAs.

2.7 Lentiviral infection

The recombinant lentiviruses LV3(H1/GFP&Puro) were synthesized by GenePharma Company (Shanghai, CHN). The packaged lentiviruses included miR-335-3p mimics (5'-TTTTTCATTATTGCTCCTGACC-3'), miR-335-3p inhibitors (5'-GGTCAGGAGCAATAATGAAAAA-3'), or miR-NC (5'-TTCTCCGAACGTGTCACGT-3'). For mBMSCs transfection, lentiviruses at a multiplicity of infection of 100 were added to the culture medium with 8 mg/mL polybrene for 12 h when mBMSCs achieved 50% confluence followed by selection with 5 μg/mL puromycin (Sigma-Aldrich, MO, USA) for 3 days. The transfection efficiency was confirmed by GFP fluorescence signal under an inverted fluorescence microscopy.

2.8 Reporter vector construction and dual-luciferase reporter assay

The 3'-untranslated region (UTR) of Aplnr containing the predicted miR-335-3p binding sites was inserted into pEZX-MT06 vector (GeneCopoeia, MD, USA) to form a wild-type APLNR (APLNR-WT) luciferase reporter APLNR-WT. The 3'-UTR of Aplnr containing the mutated miR-335-3p binding sites was inserted into pEZX-MT06 vector to form a mutant-type APLNR (APLNR-MT) luciferase reporter plasmid. The luciferase reporter assays were performed according to the manufacturer's protocol. Briefly, the mBMSCs were cultured in a 24-well plate until reaching 50% confluence. 1 μg of APLNR-WT reporter plasmids, APLNR-MT reporter plasmids, or NC reporter plasmids were mixed with Lipofectamine™ 3000 Reagent (Invitrogen, MA, USA) and P3000™ Reagent (Invitrogen, MA, USA) diluted in Opti-MEM™ medium (Gibco, NY, USA) and incubated for 15 min at room temperature. Then, 100 nM of miR-NC or miR-335-3p mimics were mixed with Lipofectamine™ 3000 Reagent diluted in Opti-MEM™ medium and incubated for 15 min at room temperature. The plasmid mixture and miRNA mixture were incubated with mBMSCs for 2 days. After that, the luciferase activity was measured by the Dual-Luciferase Reporter Assay System. All luciferase values were normalized to Renilla luciferase.

2.9 Transfection of miR-335-3p inhibitor to exosomes

O-Exos were loaded with miR-335-3p inhibitor (GenePharma, Shanghai, CHN) (O-Exos+anti-miR-335) or negative control (GenePharma, Shanghai, CHN) (O-Exos+NC) using an Exo-Fect™ Exosome Transfection Kit (System Biosciences, CA, USA) according to the manufacturer's instructions. In brief, O-Exos and miR-335-3p inhibitor or negative control were mixed with Exo-Fect solution followed by incubation in a shaker at 37 °C for 10 min. Then, the ExoQuick-TC reagent was added to the transfected exosomes suspension to stop the reaction. After 30 min of incubation at 4 °C, the sample was centrifuged at 14,000 rpm for 3 min to precipitate exosomes, which was then resuspended in 200 μL PBS.

2.10 In vitro osteogenic differentiation assays

P-Exos, O-Exos, or O-Exos+anti-miR-335-3p were added to the OM depleted of exosomes to prepare a medium containing 50 μg/μL of P-Exos, O-Exos, or O-Exos+anti-miR-335-3p, which were then used to culture the OVX mBMSCs separately with the medium refreshed every 3 days. Sham mBMSCs or OVX mBMSCs treated with culture medium depleted of exosomes were used as the control group. After incubation for 3 and 7 days, alkaline phosphatase (ALP) staining and ALP activity quantification, quantitative real-time polymerase chain reaction (qRT-PCR), and western blotting were used to evaluate the osteogenic ability of OVX mBMSCs treated with exosomes. The detailed procedures were described in the following sections.

2.11 ALP staining and activity quantification

ALP staining was conducted using an NBT/BCIP staining kit (Beyotime Biotechnology, Shanghai, CHN) after the cells rinsed with PBS and fixed in 95% ethanol for 30 min. For ALP activity quantification assay, cells were lysed and centrifuged at 14,000 rpm for 20 min to obtain the supernatants. Then, ALP activity quantification assay was conducted using an Alkaline Phosphatase Assay Kit (Beyotime Biotechnology, Shanghai, CHN). The results were normalized to total protein which was quantified by the Piece BCA protein assay kit (Thermo Scientific, MA, USA). All the procedures were performed as per the manufacturer's protocols.

2.12 qRT-PCR

Total RNA of the cells and exosomes were extracted with TRIzol reagent (Invitrogen, MA, USA) and miRNeasy Maxi Kit (QIAGEN, Dusseldorf, Germany) respectively. The quantitative analysis of mRNA was performed using PrimeScript RT Reagent Kit (TAKARA, Shiga, Japan). Briefly, cDNAs were obtained by reverse transcription of 500 ng RNAs at 37 °C for 15 min, 85 °C for 5 s, and then 4 °C for 2 h. Next, gene expression was analyzed using a 7500 real-time PCR detection system (Applied Biosystems, MA, USA) with a Power SYBR Green Master Mix (Roche, Basel, Switzerland) at the following settings: 95 °C for 10 min, 40 cycles of 95 °C for 15 s, and 60 °C for 1 min.

The miRNA determination was performed using a poly-A polymerase tailing PCR kit and stem-loop PCR kit according to the manufacturer's instructions. For poly-A polymerase tailing PCR, 1,000 ng cellular RNAs or 100 ng exosomal RNAs were reverse transcribed to cDNAs using miDETECT A Track miRNA qRT-PCR Starter Kit (RiboBio, Guangdong, China) under the following steps: 37 °C for 1 h to add poly-A tail, then the reverse transcription was performed at 42 °C for 1 h and incubated at 72 °C for 10 min. The real-time PCR assay after poly-A tailing was performed under the following conditions: 95 °C for 10 min, 40 cycles of 95 °C for 2 s, 60 °C for 20 s, and 70 °C for 10 s. For stem-loop PCR, 1,000 ng cellular RNAs or 100 ng exosomal RNAs were reverse transcribed to cDNAs using Bulge-Loop miRNA qRT-PCR Starter Kit (RiboBio, Guangdong, China) according to the following settings: 42 °C for 60 min, 70 °C for 10 min, and store at 4 °C. The settings of the real-time PCR assay after stem-loop reverse transcription were the same as those of poly-A polymerase tailing PCR.

The internal standards for mRNA and miRNA were glyceraldehyde-3-phosphate dehydrogenase (GAPDH) and U6 respectively. The primers were synthesized by Sangon Biotech Co., Ltd. (Shanghai, China) and RiboBio Co., Ltd., separately, and the sequences were listed in Tabel 1. The results were analyzed with the $2^{-\Delta\Delta C_t}$ relative expression method.

2.13 Western blotting

Firstly, total protein of cells or exosomes was extracted with ice-cold radioimmunoprecipitation assay buffer (RIPA) containing protease inhibitor cocktail. The lysis solution was then

Table 1 Sequences of the primers used for qRT-PCR

Gene	Forward (5′–3′)	Reverse (5′–3′)
Gapdh	TCACTCAAGATTGTCAGCAA	AGATCCACGACGGACACATT
Alp	TGACCTTCTCTCCTCCATCC	CTTCCTGGGAGTCTCATCCT
Runx2	TAAGAAGAGCCAGGCAGGTG	TGGCAGGTACGTGTGGTAGT
Ocn	TGCTTGTGACGAGCTATCAG	GAGGACAGGGAGGATCAAGT
Aplnr	TCGGCTAAGGCTGCGAGTC	CGTCTGTGGAACGGAACAC
miR-335-3p	UUUUUCAUUAUUGCUCCUGACC	UCAGGAGCAAUAAUGAAAAAUU
U6	CTCGCTTCGGCAGCACA	AACGCTTCACGAATTTGCGT

centrifuged at 14,000 rpm for 15 min. Protein concentration was determined by the Pierce BCA protein assay kit (Thermo Scientific, MA, USA). Then, the total protein was separated in a 10% SDS-PAGE gel at 100 V voltage followed transferring to a polyvinylidene difluoride membrane (Bio-Rad, CA, USA). Subsequently, the membrane was washed in 1×Tris-HCl buffer (TBS) with Tween-20 (TBST) three times, and then blocked with 10% fat-free milk dissolved in TBST for 2 h. After that, the membrane was incubated with the primary antibody (diluted at 1:1,000) at 4 °C overnight, followed by incubation with the second antibody (diluted at 1:10,000) at 4 °C for 1 h on a shaker. Finally, the bands were visualized by an ECL kit (CoWin Biotech, China). Except for the exosomal markers, the following antibodies were used: GAPDH (HX1832, 1:5,000, Huaxingbio, Beijing, China) and RUNX2 (12556, 1:1,000, Cell Signaling Technology, MA, USA).

2.14　Injection of exosomes *in vivo*

Twelve weeks after the OVX or Sham operation, the mice were randomly divided into four groups: Sham+PBS, OVX+PBS, OVX+P-Exos, and OVX+O-Exos. 100 μg of P-Exos or O-Exos in 200 μL of PBS or an equal volume of PBS was injected intravenously via the tail vein every 3 days. After 8 times of injection, the mice were sacrificed and the heart, lung, spleen, kidneys, liver, and femurs were harvested for further analysis.

　　To investigate the therapeutic effect of exosomes transfected with miR-335-3p inhibitor, the sham mice and OVX mice were also randomly divided into four groups: Sham+PBS, OVX+PBS, OVX+O-Exos+NC, and OVX+O-Exos+anti-miR-335-3p. The injection strategy and samples harvest were the same with that mentioned above.

2.15　Distribution of exosomes *in vivo*

The exosomes were first labeled with 3,3'-dioctadecyloxacarbocyanine perchlorate (DiR, KeyGen Biotech, Jiangsu, China) according to the manufacturer's protocol. Briefly, exosomes were incubated with DiR solution for 30 min followed by ultracentrifugation at 100,000*g* for 70 min to remove the free DiR. The labeled exosomes were injected into eight-week-old female BALB/c mice intravenously (100 μg of exosomes in 200 μL PBS/mouse) via the tail vein. Then, 12, 24, and 48 h after injection of exosomes, mice were sacrificed, and the heart, lung, spleen, kidneys, liver, and femurs were collected. The fluorescence distribution was observed by IVIS Lumina Series III (PerkinElmer, MA, USA), and the intensity of fluorescence was quantified using the IVIS® Spectrum system and Living Image Software (PerkinElmer, MA, USA).

2.16　Micro-computed tomography (micro-CT) and bone morphometric analyses

The femurs were scanned by a high-resolution Inveon micro-CT (Siemens, Berlin, Germany) with the settings as follows: 60 kV

X-ray voltage, 220 μA node current, and 1,500 ms exposure time for each of the 360 rotational steps. The region of interest (ROI) was set based on a previous literature [22]. Then, three-dimensional (3D) images were reconstructed with the multimodal 3D visualization software. To evaluate the bone morphology and bone mineral density (BMD) changes, the following indications were calculated by the Inveon Research Workplace software (Siemens, Berlin, Germany): BMD, bone volume/total volume (BV/TV), bone surface area/bone volume (BS/BV), trabecular number (Tb.N), trabecular thickness (Tb.Th), and trabecular spacing/separation (Tb.Sp).

2.17　Histological and tartrate-resistant acid phosphatase (TRAP) staining

All the harvested organs were fixed in 4% paraformaldehyde for two days. Sections of the organs (heart, lung, spleen, kidneys, and liver) embedded in paraffin were cut, deparaffinized, dehydrated, and stained with hematoxylin and eosin (H&E) and Masson trichrome to observe whether there were obvious lesions in these organs.

　　After decalcification with 0.5 M ethylene diamine tetraacetic acid (EDTA) in PBS for 4 weeks, the femurs were dehydrated and embedded in paraffin. Sections were then obtained and stained with H&E, Masson trichrome, and TRAP.

2.18　Immunohistochemistry (IHC) staining

Firstly, sections of femurs were deparaffinized in xylene and dehydrated in series of ethanol, followed by recovery of antigens in Tris/EDTA buffer at 95 °C for 10 min. Then, endogenous peroxidase was inactivated, followed by blocking with goat serum at room temperature for 30 min. Sections were then incubated with osteocalcin (OCN) primary antibody (GB11233, 1:400, Servicebio, China) at 4 °C overnight. Subsequently, the sections were incubated with secondary antibody, visualized with diaminobezidin (DAB), and counterstained with hematoxylin.

2.19　Statistical analysis

The data were expressed as the means ± standard deviation (SD). When the differences between two groups being analyzed, a two-sided Student's *t*-test was used, while a one-way analysis of variance (ANOVA) with the Turkey's test was used to analyze differences between more than two groups. $P < 0.05$ was considered statistically significant. All results were analyzed using the Prism9.0 software (GraphPad, CA, USA).

3　Results

3.1　Characterization of hASCs derived exosomes

Cup-shaped vesicles in the extracted exosome samples with a diameter of about 100 nm (Fig. 1(a)) were observed under TEM images, which were in accordance with the typical shape of the
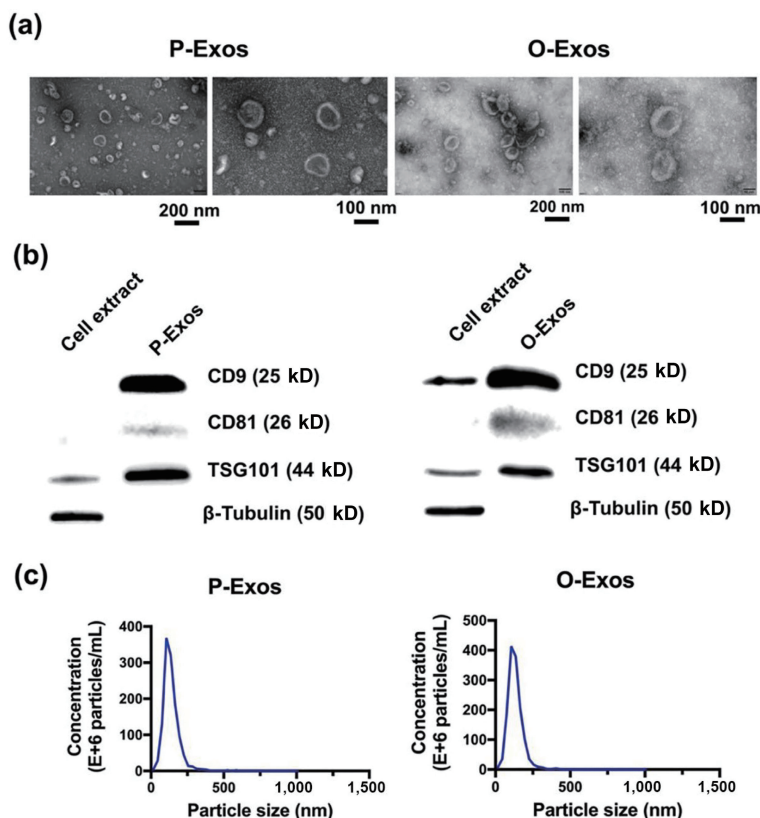
Figure 1 Characterization of hASC-derived exosomes. (a) P-Exos and O-Exos under TEM field of view. (b) Western blotting analysis of the exosomal markers, β-tubulin was a negative marker protein. (c) The size distribution of P-Exos and O-Exos measured by nanoparticle tracking analysis.

exosomes. Western blotting analysis showed that exosome-specific markers CD9, CD81, and TSG101 were positively expressed in exosome samples, while exosome-negative marker β-tubulin was barely detected (Fig. 1(b)). NTA analysis revealed that the particle diameter of the P-Exos sample mainly distributed in the range of 77–180 nm, and the mean size ± SD of P-Exos was 132.2 ± 54.3 nm. The particle diameter of the O-Exos sample was mainly distributed in the range of 81–192 nm, and the mean size ± SD of O-Exos was 136.4 ± 56.8 nm (Fig. 1(c)). The above results showed that the exosomes had been successfully extracted.

3.2 Internalization of exosomes by mBMSCs

To determine whether the exosomes could be internalized by mBMSCs, PKH26 labeled P-Exos and O-Exos were co-cultured with mBMSCs. Red fluorescence detected in mBMSCs gradually accumulated from 12 to 72 h, which meant that an increasing number of P-Exos or O-Exos was internalized by mBMSCs as time passed. The slightly stronger fluorescence intensity in mBMSCs incubated with O-Exos indicated that more O-Exos were likely to be internalized by mBMSCs compared with P-Exos (Figs. 2(a) and 2(b)). The reason may be that those pre-osteogenic differentiated ASC-derived exosomes express more surface ligands that can be identified by the bone marrow derived stem cells (i.e., mBMSCs).

3.3 O-Exos rather than P-Exos rescued osteogenic differentiation of OVX mBMSCs *in vitro*

To verify the effect of exosomes derived from hASCs on the osteogenic differentiation of OVX mBMSCs, P-Exos or O-Exos were co-cultured with OVX mBMSCs. A stronger ALP staining of Sham mBMSCs compared with OVX mBMSCs indicated the impaired osteogenic differentiation of mBMSCs from OVX mice (Fig. 3(a)). In addition, the intensity of ALP staining of OVX mBMSCs was significantly enhanced after co-culture with
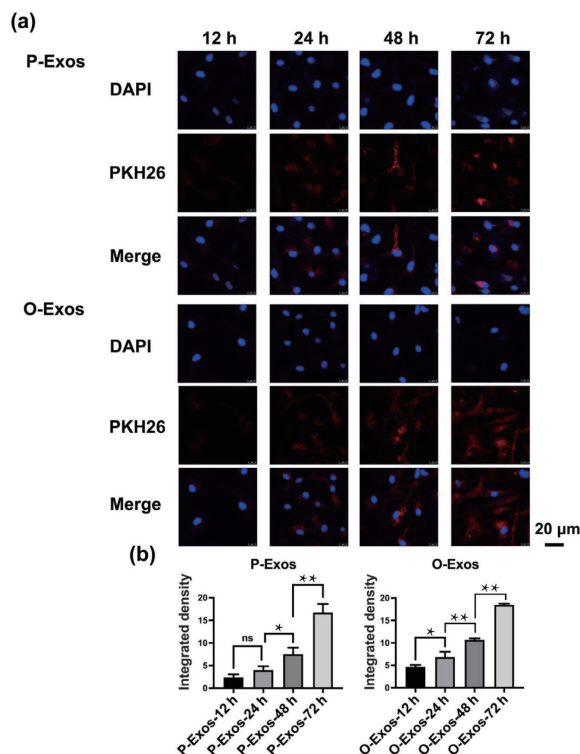

Figure 2 P-Exos and O-Exos were internalized by mBMSCs. (a) Microscopic images of PKH26 (red) positive exosomes and DAPI (blue). (b) Quantitative analysis of PKH26 fluorescence signal. The data are presented as mean ± SD, *$P < 0.05$, and **$P < 0.01$.

O-Exos according to ALP activity analysis ($P < 0.01$), while no significant difference was detected between OVX mBMSCs with or without P-Exos (Fig. 3(b)). Furthermore, the results of qRT-PCR showed that O-Exos enhanced the expression of osteogenic
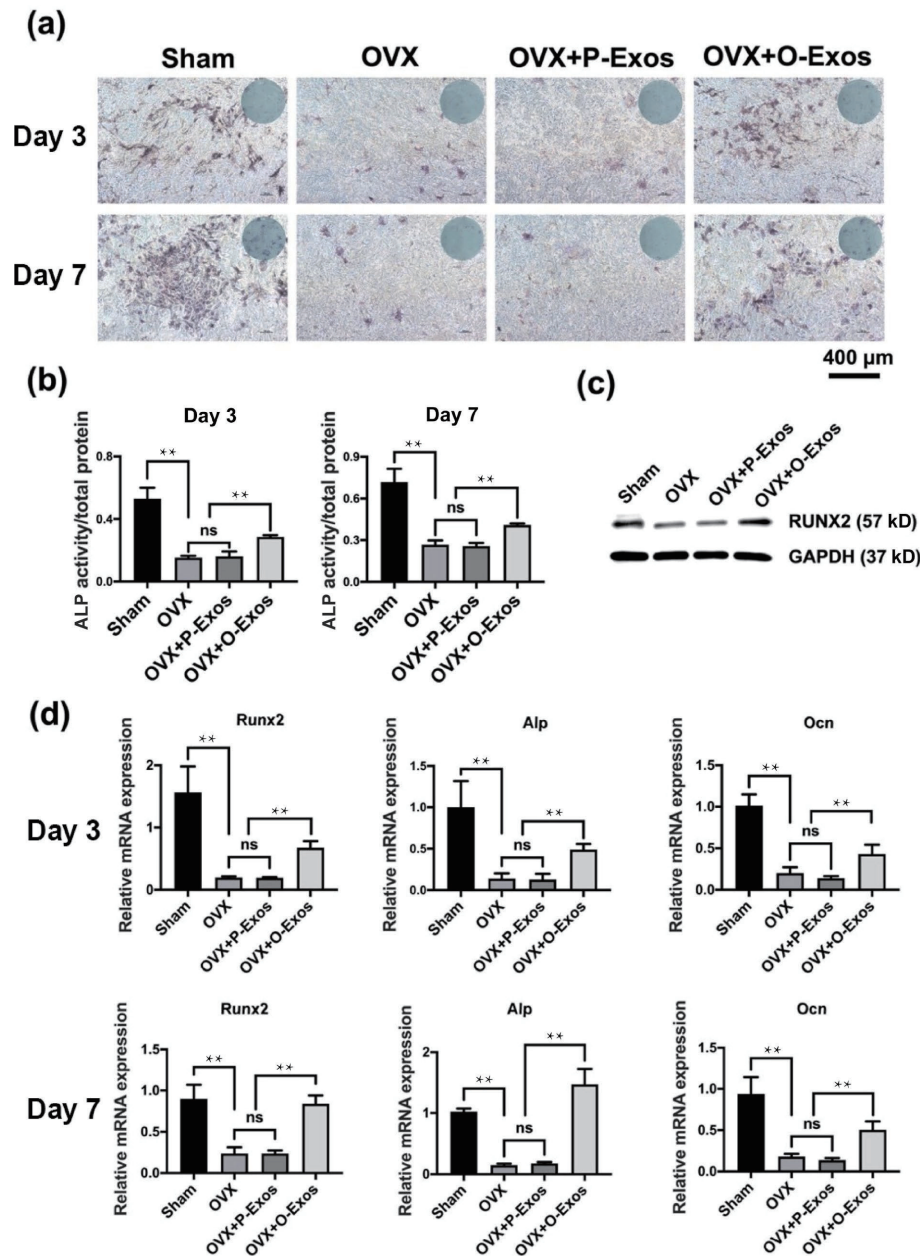
Figure 3 O-Exos rescued osteogenic differentiation of OVX mBMSCs *in vitro*. (a) ALP staining on day 3 and day 7. (b) ALP activity quantitative analysis on day 3 and day 7. (c) Western blotting analysis of RUNX2, GAPDH as an internal reference. (d) Expression of osteogenic genes Runx2, Alp, and Ocn in mBMSCs cultured with P-Exos or O-Exos on day 3 and day 7. The data are presented as mean ± SD, *$P < 0.05$, and **$P < 0.01$.

genes (i.e., Alp, Ocn, and Runx2) ($P < 0.01$) (Fig. 3(d)). The results of western blotting also confirmed that the protein expression of RUNX2 in OVX mBMSCs was significantly upregulated when treated with O-Exos (Fig. 3(c)). Collectively, O-Exos could rescue the osteogenic ability of OVX mBMSCs, while P-Exos had no obvious effect.

3.4 Biodistribution of exosomes *in vivo*

To analyze the distribution of exosomes after injection intravenously, DiR-labeled P-Exos or O-Exos were injected through the tail vein. As shown in Fig. S1 in the Electronic Supplementary Material (ESM), P-Exos or O-Exos were mainly concentrated in the liver, followed by the spleen. Fluorescence signal could also be observed in the femurs, but not as strong as the first two. After 12 h, the fluorescence signal started to decline in liver and kidney, which also decreased in spleen after 24 h. Nevertheless, no significant decrease in fluorescence signal was observed in the femurs from 12 to 48 h. These findings might be

explained by a re-biodistribution and metabolic degradation of exosomes by these organs.

3.5 O-Exos and P-Exos ameliorated osteoporosis in OVX mice

In this study, an osteoporotic model was established by bilateral ovariectomies. Micro-CT images and bone morphometric quantification results showed that the femoral trabeculae harvested from OVX mice 3 months after surgery were significantly sparser than those in the Sham group ($P < 0.01$) (Figs. S2(a) and S2(b) in the ESM). Therefore, the osteoporotic model was successfully constructed. To clarify the therapeutic effect of exosomes on osteoporosis, P-Exos or O-Exos were injected intravenously into OVX mice by the tail vein. The safety of P-Exos or O-Exos was evaluated and ensured, as the injection of either kind of exosomes did not cause any pathological changes of heart, lung, spleen, liver, and kidneys (Fig. S3(a) in the ESM). Micro-CT revealed that the trabecular structure of femurs of OVX mice

injected with O-Exos was denser than that of OVX mice injected with PBS (Fig. 4(a)), which was confirmed by a substantial increase of BMD in group O-Exos ($P < 0.05$) (Fig. 4(b)(i)). Although the BMD after injection of O-Exos was slightly higher than that of P-Exos, there was no significant statistical difference between them (Fig. 4(b)(i)). Bone morphometric quantifications analysis demonstrated that injection of P-Exos or O-Exos resulted in significant increases in BV/TV, Tb.Th, and Tb.N ($P < 0.05$ or $P < 0.01$) (Figs. 4(b)(ii)–4(b)(iv)), as well as significant decreases in BS/BV and Tb.Sp compared to that of PBS group ($P < 0.05$ or $P < 0.01$) (Figs. 4(b)(v) and 4(b)(vi)). Similar to the BMD, the average value of BV/TV, Tb.Th, and Tb.N (Figs. 4(b)(ii)–4(b)(iv)) in OVX+O-Exos group was slightly higher and the mean value of BS/BV and Tb.Sp (Figs. 4(b)(v) and 4(b)(vi)) in OVX+O-Exos group was slightly lower than that in OVX+P-Exos group, but there was no significant difference between the two groups. The results of histological analyses were in consistence with those of

micro-CT scanning. While the number of trabecular bones decreased and the gap between trabecular bones increased in the control OVX mice, the number of trabecular bones increased in groups of P-Exos and O-Exos injection (Fig. 4(c)). TRAP staining and IHC staining of OCN indicated that injection of P-Exos and O-Exos caused a decrease in osteoclast number and an increase in osteoblast number in trabecular bones, respectively (Fig. 4(d)).

3.6 Distinct levels of miRNA expression in O-Exos and P-Exos

To explore the mechanism of O-Exos in promoting osteogenic differentiation and ameliorating osteoporosis, small RNA sequencing and bioinformatic analyses were conducted. A total of 2,684 miRNA expressions in P-Exos, O-Exos-7d, and O-Exos-14d were detected. There were 16 upregulated differentially expressed miRNAs and 24 downregulated miRNA when comparing O-Exos-7d with P-Exos, while 41 upregulated miRNAs and 31
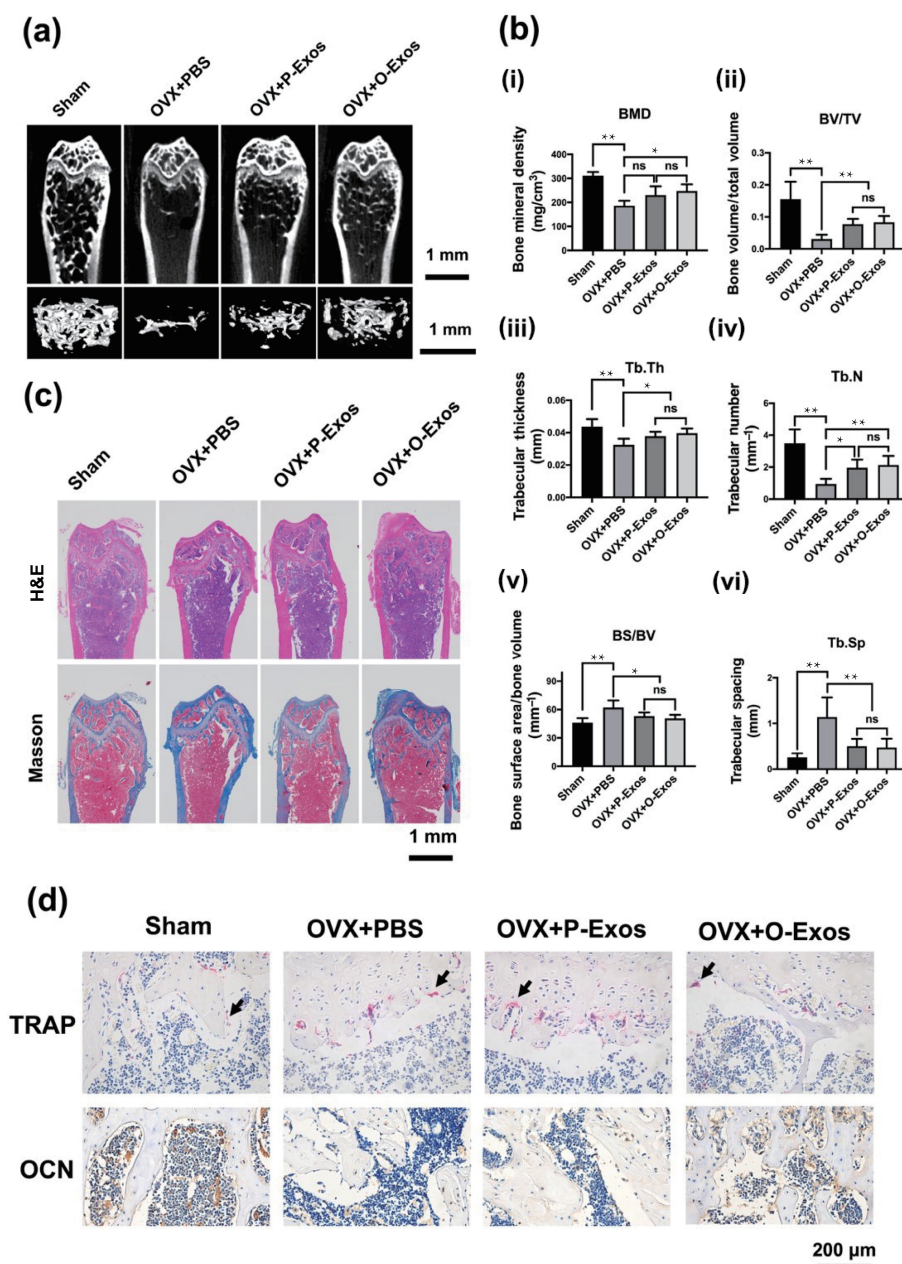

Figure 4 P-Exos and O-Exos ameliorated osteoporosis in OVX mice. (a) Micro-CT images and 3D reconstructed images of mouse femurs after treatment of P-Exos or O-Exos. (b) BMD and bone morphometric analyses, including BV/TV, BS/BV, Tb.N, Tb.Th, and Tb.Sp of mouse femurs after treatment of P-Exos or O-Exos. (c) H&E and Masson staining of mouse femurs after treatment with P-Exos or O-Exos. (d) TRAP staining and OCN immunostaining of mouse femurs after treatment of P-Exos or O-Exos. The data are presented as mean ± SD, *$P < 0.05$, and **$P < 0.01$.

downregulated miRNAs when comparing O-Exos-14d with P-Exos (Fig. 5(a)). Differences in miRNA expression among P-Exos, O-Exos-7d, and O-Exos-14d are shown in the Venn diagram (Fig. 5(b)). Expression heat maps based on normalized $\log_2$RPKM (reads per kilobase of transcript per million mapped reads) of representative differentially expressed miRNAs among P-Exos, O-Exos-7d, and O-Exos-14d are shown in Fig. 5(c). Among all differentially expressed miRNAs, there were only four miRNAs, miR-93-3p, miR-501-3p, miR-490-3p, and miR-335-3p downregulated both in O-Exos-7d and O-Exos-14d compared with those in P-Exos. Meanwhile, there were no miRNAs expressed at significantly higher levels in both O-Exos-7d vs. P-Exos and O-Exos-14d vs. P-Exos. Therefore, these four miRNAs were selected as candidate miRNAs to further explore the mechanism by O-Exos to promote osteogenic differentiation.

3.7 Validation of miRNA differential expression in hASCs and exosomes during osteogenic differentiation

The expression of miRNAs in hASCs and exosomes was further verified by qRT-PCR. The results of poly-A polymerase tailing method showed that the expression of miR-93-3p, miR-501-3p, miR-490-3p, and miR-335-3p was all decreased significantly during the process of osteogenic differentiation (OM-7d and OM-14d), while the decrease of miR-335-3p was the most obvious ($P < 0.01$) (Fig. 5(d)). After that, qRT-PCR using the stem-loop method also verified the expression trend of miR-335-3p ($P < 0.01$) (Fig. 5(e)). Therefore, miR-335-3p was ultimately adopted as the key miRNA in exosomes promoting osteogenesis *in vitro* and *in vivo*.

3.8 miR-335-3p inhibited osteogenic differentiation of mBMSCs *in vitro*

To investigate the role of miR-335-3p in the osteogenic differentiation of mBMSCs, miR-335-3p mimics, miR-335-3p inhibitors, or miR-NC was transfected into mBMSCs respectively through lentiviral infection. The qRT-PCR showed that the expression level of miR-335-3p increased approximately 3.6 times after transfection of miR-335-3p mimics, while reduced to about 60% after transfection of miR-335-3p inhibitors ($P < 0.01$) (Fig. 6(d)).
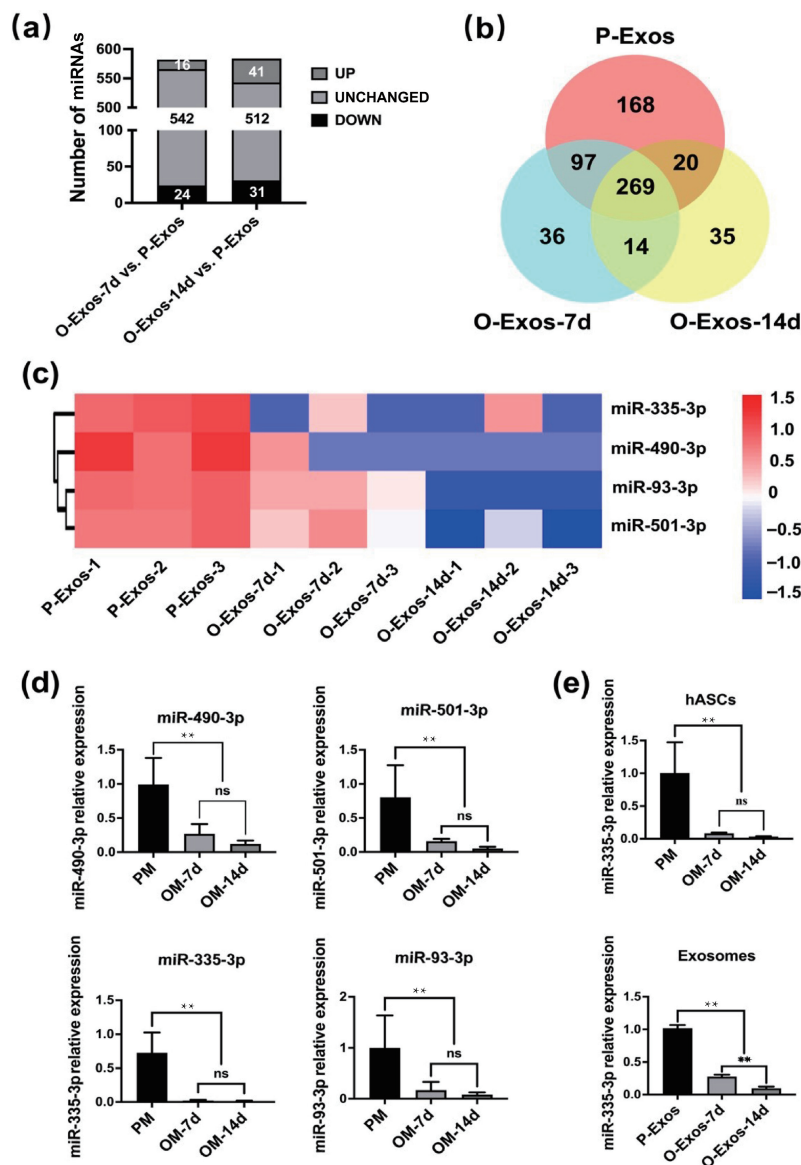

Figure 5 miRNA sequencing and validation in hASCs and exosomes. (a) Differentially expressed miRNAs between O-Exos-7d vs. P-Exos and O-Exos-14d vs. P-Exos. (b) Differences in miRNA expression among P-Exos, O-Exos-7d, and O-Exos-14d are shown in the Venn diagram. (c) Expression heat maps of miRNA expression among P-Exos, O-Exos-7d, and O-Exos-14d. (d) qRT-PCR validation of miRNA expression during osteogenic differentiation of hASCs using a poly-A polymerase tailing PCR kit. (e) Validation of miR-335-3p expression during osteogenic differentiation of hASCs and exosomes using stem-loop PCR. The data are presented as mean ± SD, *$P < 0.05$, and **$P < 0.01$.

While ALP staining of miR-335-3p mimics-transfected mBMSCs was lighter than that of miR-NC, the staining was significantly darker after transfection of miR-335-3p inhibitors (Fig. 6(a)) no matter in PM or OM. Similar results were obtained by ALP activity analysis ($P < 0.01$) (Fig. 6(b)). The relative expression of Alp, Runx2, and Ocn genes in the miR-335-3p
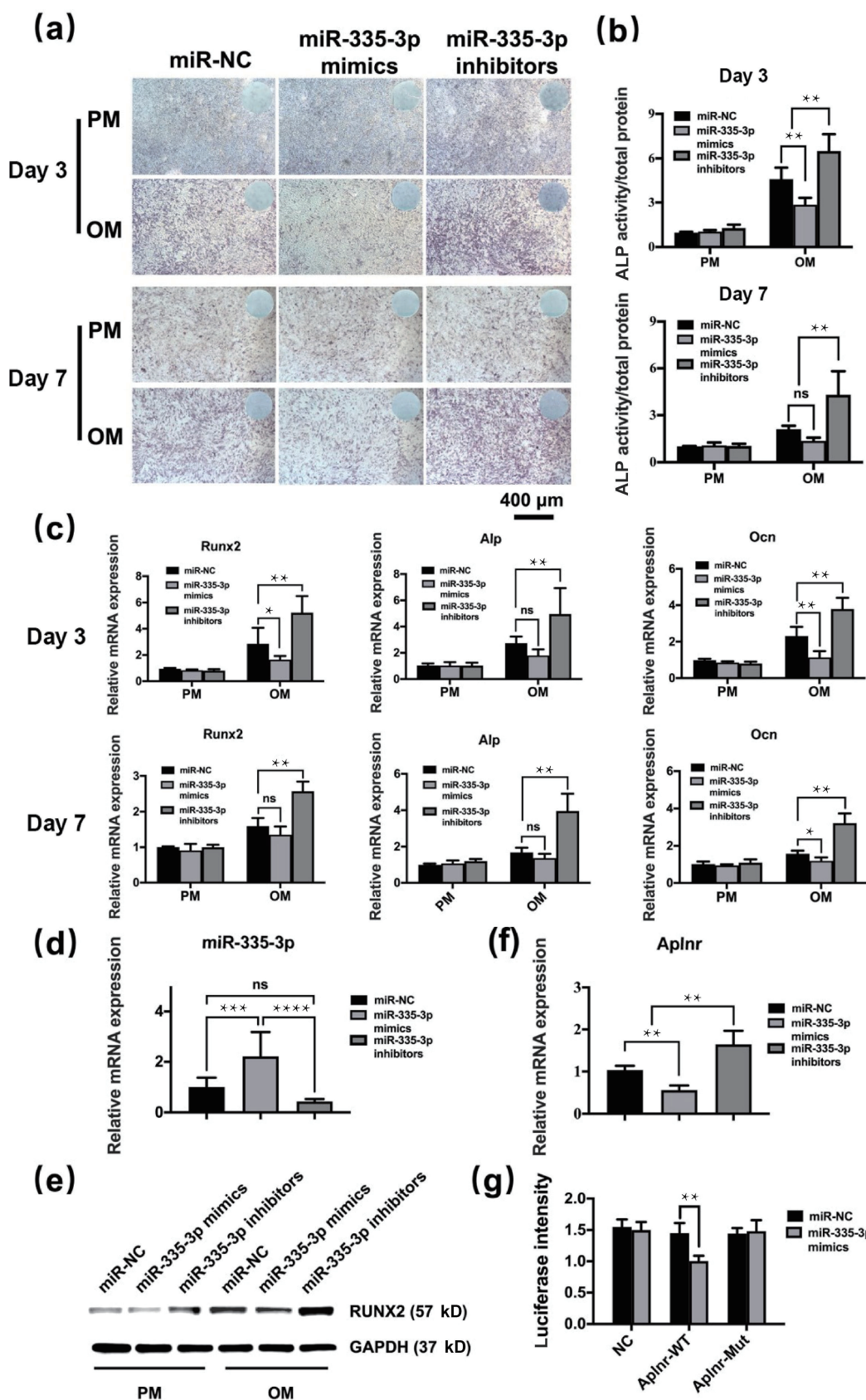

Figure 6 Inhibition of miR-335-3p expression promoted mBMSCs osteogenic differentiation. (a) ALP staining on day 3 and day 7. (b) ALP activity quantitative analysis on day 3 and day 7. (c) Expression of osteogenic genes Runx2, Alp, and Ocn in mBMSCs transfected with miR-335-3p mimics or inhibitors on day 3 and day 7. (d) qRT-PCR validation of miR-335-3p expression after transfection with lentivirus. (e) Western blotting analysis of RUNX2, GAPDH as an internal reference. The data are presented as mean ± SD, *$P < 0.05$, and **$P < 0.01$. (f) qRT-PCR validation of Aplnr after transfection with lentivirus. (g) Luciferase activity of Aplnr-WT and Aplnr-Mut after transfection with miR-335-3p mimics and miR-NC respectively.

inhibitors group significantly increased, while decreased in the miR-335-3p mimics group (Fig. 6(c)) ($P < 0.01$). Similar results were observed in protein expression of RUNX2 by western blotting (Fig. 6(e)). These results indicated that miR-335-3p played a negative regulatory role in the osteogenic differentiation of mBMSCs.

3.9 miR-335-3p regulated osteogenic differentiation of mBMSCs by targeting Aplnr

To explore the regulatory relationship between miR-335-3p and Aplnr, the mRNA expression level of Aplnr in normal mBMSCs transfected with miR-335-3p mimics or miR-335-3p inhibitors was detected. As shown by the qRT-PCR results (Fig. 6(f)), expression of Aplnr decreased markedly in mBMSCs transfected with miR-335-3p mimics, whereas increased in mBMSCs transfected with miR-335-3p inhibitors ($P < 0.01$). Then, the target relationship between miR-335-3p and Aplnr was further verified through dual-luciferase reporter assays. As depicted in Fig. 6(g), miR-335-3p mimics decreased the luciferase activity of Aplnr-WT ($P < 0.01$), and the luciferase activity of Aplnr-Mut did not change

treated with miR-335-3p mimics. These results suggested that miR-335-3p directly regulated the expression of Aplnr by targeting its 3'-UTR.

3.10 miR-335-3p inhibitor-loaded O-Exos promoted osteogenic differentiation of OVX mBMSCs *in vitro*

O-Exos loaded with or without miR-335-3p inhibitor were co-cultured with OVX mBMSCs to verify the optimized osteogenic effect of O-Exos loaded with miR-335-3p inhibitor on OVX mBMSCs. ALP staining of OVX mBMSCs was enhanced by both O-Exos and O-Exos+anti-miR-335 compared with untreated OVX mBMSCs, while the staining was stronger in group O-Exos+anti-miR-335 than that in group O-Exos. However, ALP staining in all the 3 groups was lighter than that in the Sham mBMSCs (Fig. 7(a)). The results of ALP activity assay were similar to ALP staining ($P < 0.01$) (Fig. 7(b)). Besides, O-Exos+anti-miR-335 improved the expression of osteogenic genes including Alp, Ocn, and Runx2 ($P < 0.01$) (Fig. 7(d)) and the protein expression of RUNX2 (Fig. 7(c)) compared to OVX mBMSCs treated with O-Exos.
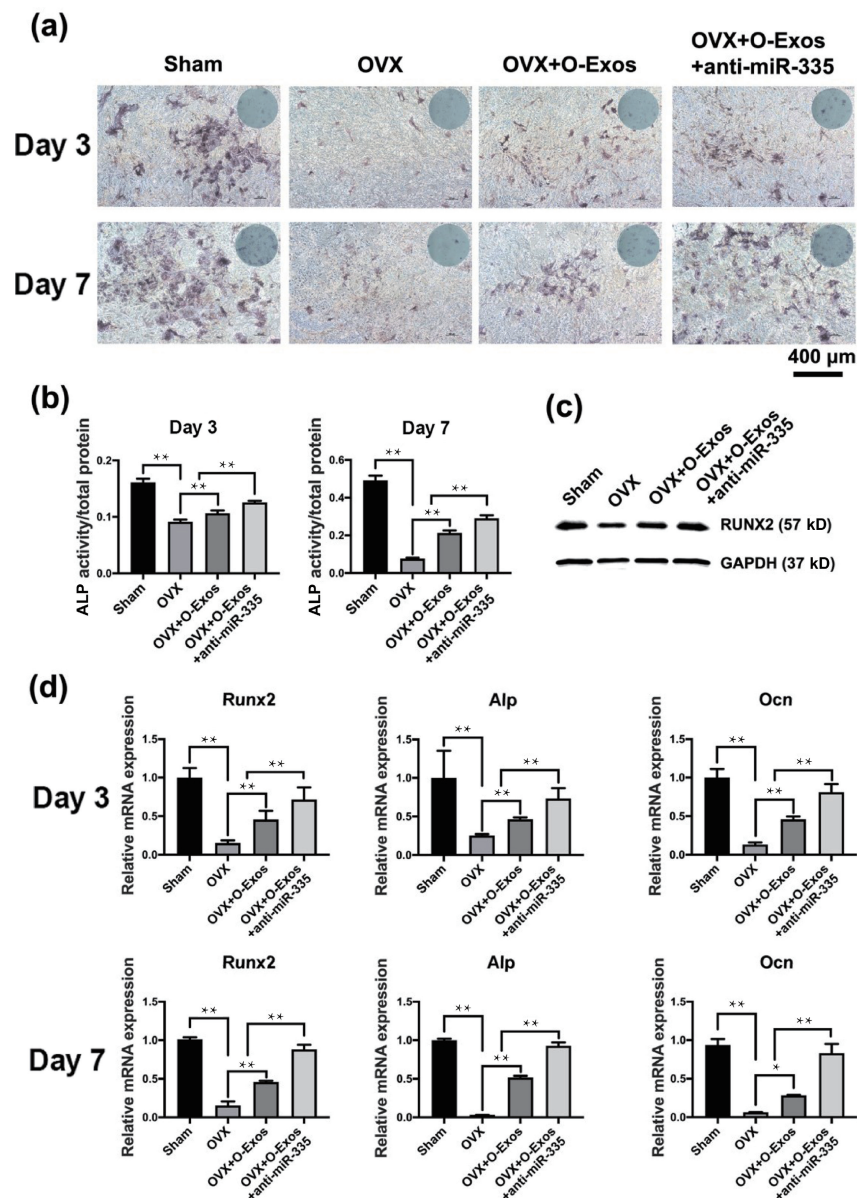

Figure 7 O-Exos loaded with miR-335-3p inhibitor promoted osteogenic differentiation of OVX mBMSCs *in vitro*. (a) ALP staining on day 3 and day 7. (b) ALP activity quantitative analysis on day 3 and day 7. (c) Western blotting analysis of RUNX2, GAPDH as an internal reference. (d) Expression of osteogenic genes Runx2, Alp, and Ocn in mBMSCs cultured with O-Exos or O-Exos+anti-miR-335 on day 3 and day 7. The data are presented as mean ± SD, *$P < 0.05$, and **$P < 0.01$.

3.11 miR-335-3p inhibitor-loaded O-Exos was more effective than O-Exos in ameliorating osteoporosis in OVX mice

To find out whether miR-335-3p inhibitor-loaded O-Exos were better than O-Exos in treating osteoporosis, O-Exos or O-Exos+anti-miR-335 were injected intravenously into OVX mice. H&E staining of heart, lung, spleen liver, and kidneys showed that the injection of O-Exos+anti-miR-335 did not cause obvious organic disease (Fig. S3(b) in the ESM). Micro-CT images revealed that the trabecular structure of femurs of group OVX+O-Exos+anti-miR-335 was significantly denser than those of group OVX+O-Exos and group OVX+PBS (Fig. 8(a)). Figure 8(b)(i) shows a substantial increase in BMD in group O-Exos+anti-miR-335 compared to those in group OVX+O-Exos and OVX+PBS ($P < 0.05$ or $P < 0.01$). Bone morphometric quantifications analysis demonstrated that the values of BV/TV and Tb.N were significantly higher in group O-Exos+anti-miR-335 than those in

group OVX+O-Exos and group OVX+PBS (Figs. 8(b)(ii) and 8(b)(iv)), while BS/BV and Tb.Sp were significantly lower ($P < 0.05$ or $P < 0.01$) (Figs. 8(b)(v) and 8(b)(vi)). The results of histological analyses were similar to the micro-CT results (Fig. 8(c)). The number of trabecular bones increased significantly in group O-Exos+anti-miR-335 compared to group O-Exos. TRAP and OCN staining (Fig. 8(d)) indicated that injection of O-Exos+anti-miR-335 reduced the numbers of osteoclasts and increased the osteoblasts numbers in trabecular bones when compared to the group O-Exos or PBS.

4 Discussion

In the current study, it was found that exosomes derived from ASCs of osteogenic commitment are capable of promoting the osteogenic differentiation of OVX mBMSCs and ameliorating the osteoporotic condition. miRNA-335-3p was identified as the key miRNA in exosomes driving the osteogenic effect, and miRNA-
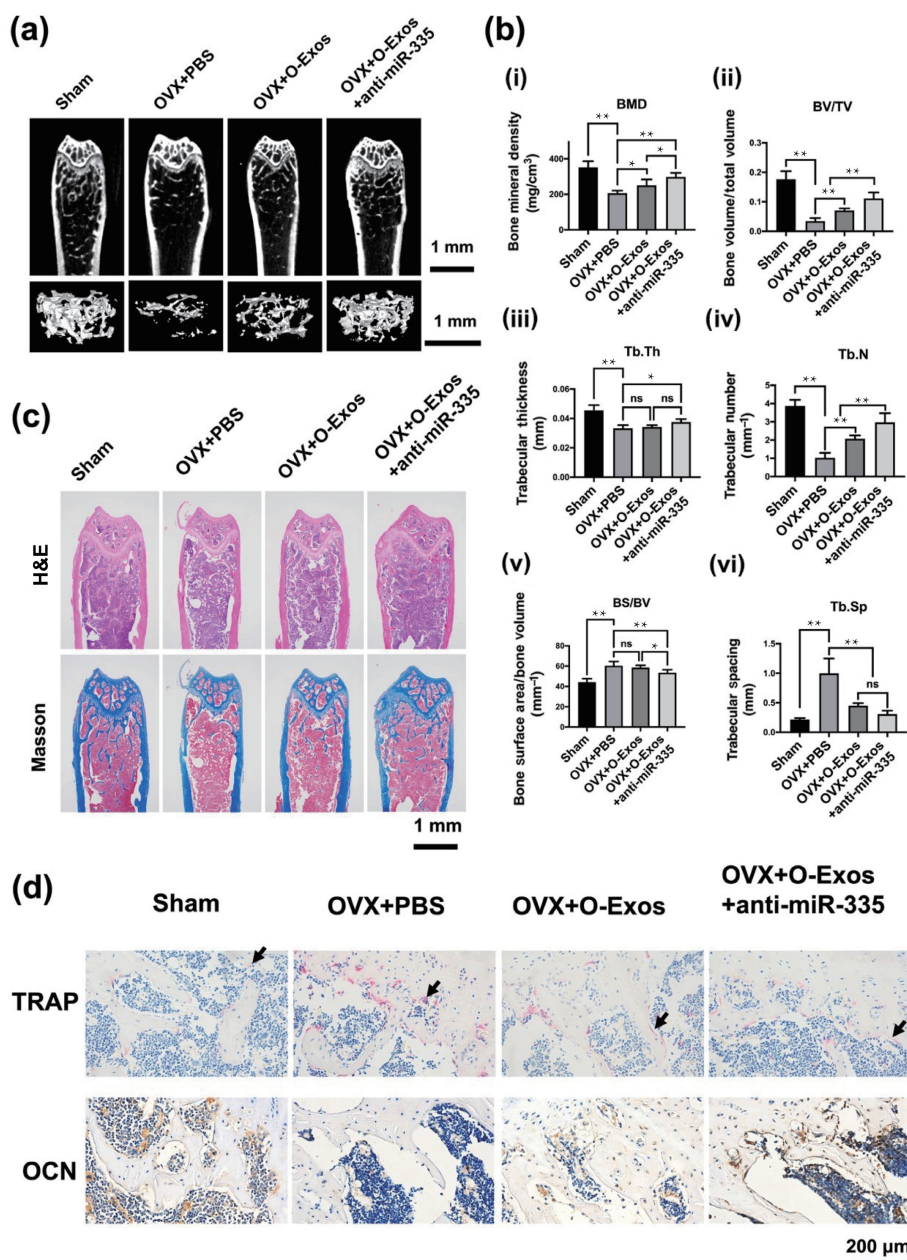

Figure 8 O-Exos+anti-miR-335 ameliorated osteoporosis in OVX mice. (a) Micro-CT images and 3D reconstructed images of mouse femurs after treatment of O-Exos or O-Exos+anti-miR-335. (b) BMD and bone morphometric analyses, including BV/TV, BS/BV, Tb.N, Tb.Th, and Tb.Sp of mouse femurs after treatment of O-Exos or O-Exos+anti-miR-335. (c) H&E and Masson staining of mouse femurs after treatment with O-Exos or O-Exos+anti-miR-335. (d) TRAP staining and OCN immunostaining of mouse femurs after treatment of O-Exos or O-Exos+anti-miR-335. The data are presented as mean ± SD, *$P < 0.05$, and **$P < 0.01$.

335-3p-inhibitor-optimized exosomes showed better effect in promoting the osteogenic differentiation of OVX mBMSCs and ameliorating osteoporosis of the OVX mice compared with the unoptimized exosomes. Therefore, this study revealed the potential of hASC-derived exosomes to treat osteoporosis *in vivo* and *in vitro*, which provides a new promising strategy to treat osteoporosis in clinic.

ASCs derived from human rather than mouse were selected in this study. The first reason is that results obtained with human-derived cells are more conducive to clinical translation. Secondly, exosomes were highly conserved among eukaryotes, which means the cargos of exosomes, such as miRNA sequences and protein amino acid sequences, were highly homologous among eukaryotes [23–25]. In addition, existing studies have verified the ability of human MSC-derived exosomes to function as therapeutic agents in animal disease models. For example, human umbilical cord mesenchymal stem cell exosomes were demonstrated to have the ability to treat skin burns and acute kidney injury in rats [26, 27]. Therefore, human ASC-derived exosomes were selected as the research object to explore the possibility of applying ASC-derived exosomes in the treatment of osteoporosis.

Osteogenic differentiation ability of BMSCs from osteoporotic rats has been confirmed to be significantly impaired [28], which might contribute to osteoporosis. Therefore, a potential treatment for osteoporosis is to restore the damaged osteogenic differentiation abilities of BMSCs [29]. For example, Pargylin, an inhibitor of lysine-specific demethylase 1 (LSD1), which could promote the osteogenic differentiation of mouse BMSCs from osteoporotic conditions, has been reported to rescue the osteoporotic condition in aged or ovariectomized mouse models [22]. In this study, we demonstrated that exosomes secreted by pre-osteogenic differentiated hASCs could rescue the osteogenic differentiation ability of OVX mBMSCs *in vitro*, which is similar with the findings of Li et al., who found that exosomes extracted from osteogenic differentiated hASCs could promote osteogenic differentiation of hBMSCs *in vitro* at all the timepoints tested (2, 4, 7, and 14 days) [30]. Besides, Liu et al. confirmed the stronger osteoinductivity of osteogenic ASC-derived exosomes on rBMSCs than non-osteoinductive ASC-derived exosomes [31]. However, the existing studies did not investigate the effect of ASC-derived exosomes on osteoporosis. In the present study, we firstly confirmed the therapeutic effect of exosomes derived from the pre-osteogenic differentiated hASCs on the osteoporosis of OVX mice. In a word, our findings indicated that hASC-derived-exosomes could rescue the osteoporotic conditions via restoring the osteogenic differentiation abilities of BMSCs. Besides, the inhibition of osteoclastogenesis by O-Exos as confirmed by TRAP staining (Fig. 4) indicated that osteoclasts may also be involved in the therapeutic effect of O-Exos on osteoporosis. Further mechanisms of how ASC-derived exosomes inhibit osteoclastogenesis will be investigated in the future studies.

Next, the mechanism of how O-Exos promote the osteogenic differentiation was clarified. Exosomes deliver proteins, nucleic acids, and other substances to target cells for signal transduction and substance transmission [32], among which, miRNAs, small noncoding RNAs regulating multiple cellular behaviors at post-transcriptional level, are one of the key functional components of exosomes [33]. So far, several exosomal miRNAs have been confirmed to have the effect of promoting osteogenic differentiation or bone formation [13, 16]. For instance, exosomes derived from BMSCs were confirmed to promote osteoblast proliferation and differentiation via delivering microRNA-150-3p [16]. In the present study, miR-335-3p was identified as the key miRNA responsible for the osteoinductivity of O-Exos based on the findings of miRNA-seq, qRT-PCR, and functional assays.

Interestingly, while most of miRNAs capable of promoting osteogenic differentiation were upregulated in the exosomes, miR-335-3p was downregulated in O-Exos in the current study. Subsequently, the mechanism by the downregulated miR-335-3p to promote osteogenic differentiation was further investigated. The result of dual-luciferase reporter assay showed that miR-335-3p directly regulated Aplnr, which was a positive regulator of osteogenic differentiation. Aplnr has been identified to activate the PI3K/AKT signaling pathway through the Elabela/Aplnr system, and the PI3K/AKT pathway was closely related to cellular osteogenic differentiation. Thus, Aplnr might promote cellular osteogenic differentiation by activating the PI3K/AKT signaling pathway [34–36]. In addition, MAPK signaling pathway might also be a signaling pathway for Aplnr to affect osteogenic differentiation. It has been reported that the expression of Aplnr could activate the MAPK signaling pathway, which could promote the differentiation of osteoblasts and inhibit osteoclasts [37, 38]. What is more, the Apelin/Aplnr system could also promote the osteogenic differentiation of BMSCs through the Wnt/β-catenin signaling pathway, which was closely related to the repairing of bone defects in patients with osteoporosis [39]. Therefore, O-Exos may affect the osteogenic differentiation of cells by regulating the expression of Aplnr in mBMSCs, and the Apelin/Aplnr system may be used as a therapeutic target for osteoporosis. Of course, this signaling pathway may not be the only mechanism by which ASC-derived O-Exos regulate osteogenic differentiation of mBMSCs. The sequencing results showed that there were other differentially expressed miRNAs between P-Exos and O-Exos, and these miRNAs may also play roles in the process of osteogenic differentiation. In addition, we found that P-Exos did not significantly promote the osteogenic differentiation of mBMSCs *in vitro*, while P-Exos played a positive role in the treatment of osteoporosis *in vivo*. The mechanism of P-Exos in the treatment of osteoporosis *in vivo* needs to be further studied.

The ability to carry various cargos, low immunogenicity, and stable bilayer phospholipid membrane structure of exosomes could be utilized to construct engineered exosomes with desirable functions. So far, several well-established strategies that allow exosomes to carry biologically active molecules (miRNAs, proteins, and so on) have been developed, such as transfection of donor cells [40], electroporation [41], or commercial exosomes transfection reagents [42, 43]. Among them, transfection of miRNA to exosomes is a convenient and efficient way. For example, Min Qiu et al. found that the exosomes transfected with miR-150-3p mimic had a stronger effect on relieving osteoporosis, while the exosomes transfected with miR-150-3p inhibitor worsened the therapeutic effect [16]. As such, based on the mechanism study, we further investigated the effect of engineered exosomes transfected with miR-335-3p inhibitor on the treatment of osteoporosis. Compared with the control unoptimized O-Exos, optimized exosomes transfected with miR-335-3p inhibitor further enhanced the osteogenic differentiation of OVX-BMSCs *in vitro* and rescued the osteoporosis *in vivo* to some extent. Therefore, injection of engineered ASC-derived exosomes transfected of miR-335-3p inhibitor may be a rationalizing and promising way to treat osteoporosis. Moreover, with the merits of ASCs (i.e., easily obtained, large amounts, and mild donor pain), ASC-derived exosomes have great translational potential. Nevertheless, the mechanism by ASC-derived exosomes to promote the osteogenic differentiation and inhibit osteoclastogenesis still needs to be investigated in the future. Besides, the subcellular distribution of exosomes, such as lysosomes, endosomes, and endoplasmic reticulum, is important to their function. For example, it has been found that the exosomes or extracellular vesicles internalized by the target cells

were colocalized with lysosomes, which resulted in the exposure of the functional cargos of exosomes in an acidification-dependent manner [44, 45]. Further study is necessary to elucidate the distribution of the exosomes. The last but not the least, large animal study is required to confirm the therapeutic effect of ASC-derived exosome on osteoporosis before clinical translation.

5 Conclusions

Exosomes secreted by pre-osteogenic differentiated hASCs could rescue the osteogenic ability of OVX mBMSCs *in vitro* and ameliorated osteoporosis in OVX mice. In addition, miR-335-3p-inhibitor-optimized exosomes had a better therapeutic effect on osteoporosis than the unoptimized exosomes. Our results indicated that the ASC-exosome-based therapy brings new possibilities for osteoporosis treatment and engineered-exosomes based on transfection of miRNAs or their inhibitors are a promising strategy to optimize the therapeutic effect of exosomes on osteoporosis.

Electronic Supplementary Material: Supplementary material (figures about the biodistribution of the exosomes, validation of osteoporotic model, and the pathological changes in organs of the mice after injection of exosomes) is available in the online version of this article at https://doi.org/10.1007/s12274-022-4554-5.

References

[1] Noel, S. E.; Santos, M. P.; Wright, N. C. Racial and ethnic disparities in bone health and outcomes in the United States. *J. Bone Miner. Res.* **2021**, *36*, 1881–1905.

[2] Zeng, Q.; Li, N.; Wang, Q. Q.; Feng, J.; Sun, D. M.; Zhang, Q.; Huang, J. Y.; Wen, Q. X.; Hu, R.; Wang, L. et al. The prevalence of osteoporosis in China, a nationwide, multicenter DXA survey. *J. Bone Miner. Res.* **2019**, *34*, 1789–1797.

[3] Lorentzon, M.; Johansson, H.; Harvey, N. C.; Liu, E.; Vandenput, L.; McCloskey, E.; Kanis, J. A. Osteoporosis and fractures in women: The burden of disease. *Climacteric* **2022**, *25*, 4–10.

[4] Brown, C. Staying strong. *Nature* **2017**, *550*, S15–S17.

[5] Compston, J. E.; McClung, M. R.; Leslie, W. D. Osteoporosis. *Lancet* **2019**, *393*, 364–376.

[6] Everts-Graber, J.; Lehmann, D.; Burkard, J. P.; Schaller, B.; Gahl, B.; Häuselmann, H.; Studer, U.; Ziswiler, H. R.; Reichenbach, S.; Lehmann, T. Risk of osteonecrosis of the jaw under denosumab compared to bisphosphonates in patients with osteoporosis. *J. Bone Miner. Res.* **2022**, *37*, 340–348.

[7] Gartlehner, G.; Patel, S. V.; Feltner, C.; Weber, R. P.; Long, R.; Mullican, K.; Boland, E.; Lux, L.; Viswanathan, M. Hormone therapy for the primary prevention of chronic conditions in postmenopausal women: Evidence report and systematic review for the US preventive services task force. *JAMA* **2017**, *318*, 2234–2249.

[8] Jiang, Y. H.; Zhang, P.; Zhang, X.; Lv, L. W.; Zhou, Y. S. Advances in mesenchymal stem cell transplantation for the treatment of osteoporosis. *Cell Proliferat.* **2021**, *54*, e12956.

[9] Mirsaidi, A.; Genelin, K.; Vetsch, J. R.; Stanger, S.; Theiss, F.; Lindtner, R. A.; von Rechenberg, B.; Blauth, M.; Müller, R.; Kuhn, G. A. et al. Therapeutic potential of adipose-derived stromal cells in age-related osteoporosis. *Biomaterials* **2014**, *35*, 7326–7335.

[10] Herberts, C. A.; Kwa, M. S. G.; Hermsen, H. P. H. Risk factors in the development of stem cell therapy. *J. Transl. Med.* **2011**, *9*, 29.

[11] Kalluri, R.; LeBleu, V. S. The biology, function, and biomedical applications of exosomes. *Science* **2020**, *367*, eaau6977.

[12] Andaloussi, S. E.; Mäger, I.; Breakefield, X. O.; Wood, M. J. A. Extracellular vesicles: Biology and emerging therapeutic opportunities. *Nat. Rev. Drug Discov.* **2013**, *12*, 347–357.

[13] Zhai, M. M.; Zhu, Y.; Yang, M. Y.; Mao, C. B. Human mesenchymal stem cell derived exosomes enhance cell-free bone regeneration by altering Their miRNAs profiles. *Adv. Sci.* **2020**, *7*, 2001334.

[14] Shi, M. M.; Yang, Q. Y.; Monsel, A.; Yan, J. Y.; Dai, C. X.; Zhao, J. Y.; Shi, G. C.; Zhou, M.; Zhu, X. M.; Li, S. K. et al. Preclinical efficacy and clinical safety of clinical-grade nebulized allogenic adipose mesenchymal stromal cells-derived extracellular vesicles. *J. Extracell. Ves.* **2021**, *10*, e12134.

[15] Qin, Y. H.; Wang, L.; Gao, Z. L.; Chen, G. Y.; Zhang, C. Q. Bone marrow stromal/stem cell-derived extracellular vesicles regulate osteoblast activity and differentiation *in vitro* and promote bone regeneration *in vivo*. *Sci. Rep.* **2016**, *6*, 21961.

[16] Qiu, M.; Zhai, S. H.; Fu, Q.; Liu, D. Bone marrow mesenchymal stem cells-derived exosomal microRNA-150-3p promotes osteoblast proliferation and differentiation in osteoporosis. *Hum. Gene Ther.* **2021**, *32*, 717–729.

[17] Mohamed-Ahmed, S.; Fristad, I.; Lie, S. A.; Suliman, S.; Mustafa, K.; Vindenes, H.; Idris, S. B. Adipose-derived and bone marrow mesenchymal stem cells: A donor-matched comparison. *Stem Cell Res. Ther.* **2018**, *9*, 168.

[18] McIntosh, K.; Zvonic, S.; Garrett, S.; Mitchell, J. B.; Floyd, Z. E.; Hammill, L.; Kloster, A.; Di Halvorsen, Y.; Ting, J. P.; Storms, R. W. et al. The immunogenicity of human adipose-derived cells: Temporal changes *in vitro*. *Stem Cells* **2006**, *24*, 1246–1253.

[19] Chen, S.; Tang, Y. M.; Liu, Y. S.; Zhang, P.; Lv, L. W.; Zhang, X.; Jia, L. F.; Zhou, Y. S. Exosomes derived from miR-375-overexpressing human adipose mesenchymal stem cells promote bone regeneration. *Cell Prolif.* **2019**, *52*, e12669.

[20] Liu, W.; Li, L. W.; Rong, Y. L.; Qian, D. F.; Chen, J.; Zhou, Z.; Luo, Y. J.; Jiang, D. D.; Cheng, L.; Zhao, S. J. et al. Hypoxic mesenchymal stem cell-derived exosomes promote bone fracture healing by the transfer of miR-126. *Acta Biomater.* **2020**, *103*, 196–212.

[21] Narayanan, K.; Kumar, S.; Padmanabhan, P.; Gulyas, B.; Wan, A. C. A.; Rajendran, V. M. Lineage-specific exosomes could override extracellular matrix mediated human mesenchymal stem cell differentiation. *Biomaterials* **2018**, *182*, 312–322.

[22] Lv, L. W.; Ge, W. S.; Liu, Y. S.; Lai, G. Y.; Liu, H.; Li, W. Y.; Zhou, Y. S. Lysine-specific demethylase 1 inhibitor rescues the osteogenic ability of mesenchymal stem cells under osteoporotic conditions by modulating H3K4 methylation. *Bone Res.* **2016**, *4*, 16037.

[23] Makino, D. L.; Baumgärtner, M.; Conti, E. Crystal structure of an RNA-bound 11-subunit eukaryotic exosome complex. *Nature* **2013**, *495*, 70–75.

[24] Makino, D. L.; Halbach, F.; Conti, E. The RNA exosome and proteasome: Common principles of degradation control. *Nat. Rev. Mol. Cell Biol.* **2013**, *14*, 654–660.

[25] Ibrahim, A.; Marban, E. Exosomes: Fundamental biology and roles in cardiovascular physiology. *Annu. Rev. Physiol.* **2016**, *78*, 67–83.

[26] Zhang, B.; Wang, M.; Gong, A. H.; Zhang, X.; Wu, X. D.; Zhu, Y. H.; Shi, H.; Wu, L. J.; Zhu, W.; Qian, H. et al. HucMSC-exosome mediated-Wnt4 signaling is required for cutaneous wound healing. *Stem Cells* **2015**, *33*, 2158–2168.

[27] Zhou, Y.; Xu, H. T.; Xu, W. R.; Wang, B. Y.; Wu, H. Y.; Tao, Y.; Zhang, B.; Wang, M.; Mao, F.; Yan, Y. M. et al. Exosomes released by human umbilical cord mesenchymal stem cells protect against cisplatin-induced renal oxidative stress and apoptosis *in vivo* and *in vitro*. *Stem Cell Res. Ther.* **2013**, *4*, 34.

[28] Huang, T. B.; Yu, Z.; Yu, Q.; Wang, Y.; Jiang, Z. W.; Wang, H. M.; Yang, G. L. Inhibition of osteogenic and adipogenic potential in bone marrow-derived mesenchymal stem cells under osteoporosis. *Biochem. Biophys. Res. Commun.* **2020**, *525*, 902–908.

[29] Chen, X. H.; Shi, Z. G.; Lin, H. B.; Wu, F.; Zheng, F.; Wu, C. F.; Huang, M. W. Resveratrol alleviates osteoporosis through improving the osteogenic differentiation of bone marrow mesenchymal stem cells. *Eur. Rev. Med. Pharmacol. Sci.* **2019**, *23*, 6352–6359.

[30] Li, W. Y.; Liu, Y. S.; Zhang, P.; Tang, Y. M.; Zhou, M.; Jiang, W. R; Zhang, X.; Wu, G.; Zhou, Y. S. Tissue-engineered bone immobilized with human adipose stem cells-derived exosomes promotes bone regeneration. *ACS Appl. Mater. Interfaces* **2018**, *10*, 5240–5254.

[31] Liu, A. Q.; Lin, D.; Zhao, H. J.; Chen, L.; Cai, B. L.; Lin, K. L.; Shen, S. G. Optimized BMSC-derived osteoinductive exosomes immobilized in hierarchical scaffold via lyophilization for bone repair through Bmpr2/Acvr2b competitive receptor-activated Smad pathway. *Biomaterials* **2021**, *272*, 120718.

[32] Liao, W.; Du, Y.; Zhang, C. H.; Pan, F. W.; Yao, Y.; Zhang, T.; Peng, Q. Exosomes: The next generation of endogenous nanomaterials for advanced drug delivery and therapy. *Acta Biomater.* **2019**, *86*, 1–14.

[33] Makarova, J.; Turchinovich, A.; Shkurnikov, M.; Tonevitsky, A. Extracellular miRNAs and cell–cell communication: Problems and prospects. *Trends Biochem. Sci.* **2021**, *46*, 640–651.

[34] Li, H.; Li, T.; Fan, J.; Li, T.; Fan, L.; Wang, S.; Weng, X.; Han, Q.; Zhao, R. C. miR-216a rescues dexamethasone suppression of osteogenesis, promotes osteoblast differentiation and enhances bone formation, by regulating c-Cbl-mediated PI3K/AKT pathway. *Cell Death Differ.* **2015**, *22*, 1935–1945.

[35] Zhao, S. J.; Kong, F. Q.; Jie, J.; Li, Q.; Liu, H.; Xu, A. D.; Yang, Y. Q.; Jiang, B.; Wang, D. D.; Zhou, Z. Q. et al. Macrophage MSR1 promotes BMSC osteogenic differentiation and M2-like polarization by activating PI3K/AKT/GSK3β/β-catenin pathway. *Theranostics* **2020**, *10*, 17–35.

[36] Fu, J. Y.; Chen, X. X.; Liu, X.; Xu, D. S.; Yang, H.; Zeng, C. T.; Long, H. B.; Zhou, C. Q.; Wu, H. D.; Zheng, G. H. et al. ELABELA ameliorates hypoxic/ischemic-induced bone mesenchymal stem cell apoptosis via alleviation of mitochondrial dysfunction and activation of PI3K/AKT and ERK1/2 pathways. *Stem Cell Res. Ther.* **2020**, *11*, 541.

[37] Zhang, J. C.; Liu, Q. M.; Fang, Z. F.; Hu, X. Q.; Huang, F.; Tang, L.; Zhou, S. H. Hypoxia induces the proliferation of endothelial progenitor cells via upregulation of Apelin/APLNR/MAPK signaling. *Mol. Med. Rep.* **2016**, *13*, 1801–1806.

[38] He, Y. D.; Li, Z.; Ding, X.; Xu, B. Y.; Wang, J. J.; Li, Y.; Chen, F. H.; Meng, F. H.; Song, W.; Zhang, Y. M. Nanoporous titanium implant surface promotes osteogenesis by suppressing osteoclastogenesis via integrin β1/FAKpY397/MAPK pathway. *Bioact. Mater.* **2022**, *8*, 109–123.

[39] Hang, K.; Ye, C. Y.; Xu, J. X.; Chen, E. M.; Wang, C.; Zhang, W.; Ni, L.; Kuang, Z.; Ying, L.; Xue, D. T. et al. Apelin enhances the osteogenic differentiation of human bone marrow mesenchymal stem cells partly through Wnt/β-catenin signaling pathway. *Stem Cell Res. Ther.* **2019**, *10*, 189.

[40] Li, Z. L.; Zhou, X. Y.; Wei, M. Y.; Gao, X. T.; Zhao, L. B.; Shi, R. J.; Sun, W. Q.; Duan, Y. Y.; Yang, G. D.; Yuan, L. J. *In vitro* and *in vivo* RNA inhibition by CD9-HuR functionalized exosomes encapsulated with miRNA or CRISPR/dCas9. *Nano Lett.* **2019**, *19*, 19–28.

[41] Liang, Y. J.; Xu, X.; Li, X. F.; Xiong, J. Y.; Li, B. Q.; Duan, L.; Wang, D. P.; Xia, J. Chondrocyte-targeted microRNA delivery by engineered exosomes toward a cell-free osteoarthritis therapy. *ACS Appl. Mater. Interfaces* **2020**, *12*, 36938–36947.

[42] del Pozo-Acebo, L.; de las Hazas, M. C. L.; Tomé-Carneiro, J.; Gil-Cabrerizo, P.; San-Cristobal, R.; Busto, R.; Garcia-Ruiz, A.; Dávalos, A. Bovine milk-derived exosomes as a drug delivery vehicle for miRNA-based therapy. *Int. J. Mol. Sci.* **2021**, *22*, 1105.

[43] Castaño, C.; Kalko, S.; Novials, A.; Parrizas, M. Obesity-associated exosomal miRNAs modulate glucose and lipid metabolism in mice. *Proc. Natl. Acad. Sci. USA* **2018**, *115*, 12158–12163.

[44] Joshi, B. S.; de Beer, M. A.; Giepmans, B. N. G.; Zuhorn, I. S. Endocytosis of extracellular vesicles and release of their cargo from endosomes. *ACS Nano* **2020**, *14*, 4444–4455.

[45] Tian, T.; Zhu, Y. L.; Hu, F. H.; Wang, Y. Y.; Huang, N. P.; Xiao, Z. D. Dynamics of exosome internalization and trafficking. *J. Cell. Physiol.* **2013**, *228*, 1487–1495.